



# Towards the Point of Care and noninvasive classification of bladder cancer from urine sediment infrared spectroscopy. Spectral differentiation of normal, abnormal and cancer patients

Monika Kujdowicz<sup>a,b</sup>, David Perez-Guaita<sup>c,d</sup>, Piotr Chłosta<sup>e</sup>, Krzysztof Okon<sup>a,\*</sup>, Kamilla Malek<sup>b,\*</sup>

<sup>a</sup> Department of Pathomorphology, Medical Faculty, Jagiellonian University Medical College, Krakow, Grzegorzewska 16, 31-531, Poland

<sup>b</sup> Faculty of Chemistry, Jagiellonian University in Krakow, Krakow, Gronostajowa 2, 30-387, Poland

<sup>c</sup> FOCAS Research Institute, Technological University Dublin, Kevin Street, Dublin 20, Ireland

<sup>d</sup> Department of Analytical Chemistry, University of Valencia, 50 Dr. Moliner Street, Research Building, 46100 Burjassot, Valencia, Spain

<sup>e</sup> Department of Urology, Medical Faculty, Jagiellonian University Medical College, Krakow, Jakubowskiego 2, 30-688, Poland

## ARTICLE INFO

### Keywords:

Point-of-Care analysis  
Bladder cancer  
Urine sediment  
Attenuated Total Reflection (ATR)  
Infrared spectroscopy

## ABSTRACT

Bladder cancer (BC) is the 9th cancer cause of death and one of most cost-intensive in the world. The diagnostic tools are still not at all satisfactory. Herein we evaluated the potential of infrared spectroscopy to detect molecular changes that precede and accompany the carcinogenesis in voided urine sediment. We collected 165 samples from patients being diagnosed for BC and measured them with attenuated total reflectance Fourier transformed infrared spectroscopy (ATR FTIR). Samples were primarily divided into three groups according to cytology that indicated the presence of normal, abnormal and cancer cells. ATR FTIR spectra of sediments were analyzed with the use of partial least square discriminant analysis (PLSDA). The 1800–750 cm<sup>-1</sup> region discriminated the three groups with selectivity and sensitivity values around 68% using cytology as a reference method. These cross-validation values (which were found significant according to a permutation test) were comparable to the sensitivity and specificity values of cytology versus the gold standard (histology). The average spectra of each class and the regression vectors of the PLS-DA indicated that an increased content of carbohydrates and nucleic acids as well as transformations of protein secondary structures were the main discriminators of healthy patients from abnormal and cancer groups. Additionally, we revised the obtained classification according to diagnosis made on histopathological assessment of bladder sections. We finally discuss the potential of the technique to be used as a Point of Care (PoC) testing tool.

## 1. Introduction

Bladder cancer (BC) constitutes significant proportion of human cancers and has a very high recurrence rate (up to 70% of cases) [1,2]. Urothelial carcinoma (BC, differentiating into urothelium) stands for about 90% of all bladder malignancies in western countries [3]. The suspicion of BC arises when a patient has hematuria and BC-positive family history or is accidentally identified with other lesions in abdomen by radiology. Currently, diagnostic methods of bladder tumor include cystoscopy coupled with biopsy and histological examination, urine cytology, molecular assays, radiological imaging [4–6]. The most common BC diagnostic methods are still histology and cytology and

immunohistochemistry if needed. Pathologists have to examine many features of cells and tissues such as architecture of the lesion, an increase of the cellular layers, cellular atypia, loss of maturation, mitotic activity, which indicate cancer; however, their interpretation is not always unequivocal. Furthermore, the biopsy sample might not contain intractable to find flat malignancy [1,7]. Urine cytology, assessing cells from the urinary tract, is noninvasive sampling but subjective, time consuming and limited by low sensitivity (ca. 70 and 30–50% for high (HG)- and low-grade (LG) carcinoma, respectively) [2,8]. HG bladder carcinoma is usually identified by the presence of a higher pleomorphism of nuclei, smaller cells with a higher nuclear to cytoplasmic ratio than in LG BC. It is relatively easy to distinguish HG BC from normal urothelial cells since

\* Corresponding authors.

E-mail addresses: [k.okon@uj.edu.pl](mailto:k.okon@uj.edu.pl) (K. Okon), [kamilla.malek@uj.edu.pl](mailto:kamilla.malek@uj.edu.pl) (K. Malek).

<https://doi.org/10.1016/j.microc.2021.106460>

Received 29 March 2021; Received in revised form 21 May 2021; Accepted 24 May 2021

Available online 26 May 2021

0026-265X/© 2021 The Author(s). Published by Elsevier B.V. This is an open access article under the CC BY license (<http://creativecommons.org/licenses/by/4.0/>).

both show markedly different morphological features like hyperchromasia, coarseness of nucleoplasm and an irregular shape of nuclei. LG BC cells are similar to normal urothelium and only few features discriminate LG BC from normal groups, e.g. reactive changes (enlarged nuclei, mitoses and nucleoli in BC) and the presence of cells fragments which mimic tumor debris. The low-grade changes, especially with papillary morphology, still might be elusive with these properties. Thus, cytology is rather a good indicator for HG and malignant cases than for patients with subtle and atypical changes in cell morphology of bladder [8]. The latter is assigned to the abnormal group whose composition is very heterogenic making difficult the unequivocal classification of the patient. Smears do not show the presence of cells morphologically classified as normal or cancerous ones and contain atypical, but negative for HG cells, or reactive cells. In addition, the background is not clear when cell fragments or leukocytes are observed. Beside urothelial cells, urine also contains matrix and cancer vesicles. Novel genetic and immunochemical tests detect extracellular vesicles, exosomes, changes in methylation status, RNA fragments (mRNA, miRNA, tRNA, lncRNA), circulating tumor and cell-free DNA (ctDNA and cfDNA, respectively) as well as changes in urinary microbiome, but they are not commonly used in screening testing due to their high cost [9–11].

This summary of diagnostic methods clearly indicates that there is still a need for searching alternative, fast, cheap, non-invasive, and objective technologies supporting the BC diagnosis. Our previous work on cell lines of BC evidenced that the discrimination and the classification of BC grade and stage is possible using vibrational spectroscopic imaging [12]. FTIR (Fourier Transform Infrared) and Raman spectroscopies reveal the chemical composition of a sample due to vibrations of components and their specific positions and intensities. Any spectral change proceeds molecular alternation induced by diseases. A potential applicability of ATR (attenuated total reflection) FTIR technique for BC classification from filtered bladder wash has been showed by Gok et al. [13]. In turn, Bensaid and co-workers have employed remote Fiber Evanescent Wave Spectroscopy (FEWS), which is a combination of ATR FTIR and fiber sensors, to analyze pre-operative and intra-operative urine [14]. IR microscopy is also a valuable tool to collect spectra from single cells. Bird and co-workers have reported IR spectra analyzed by principal component analysis (PCA) to distinguish healthy glycogen-free and -rich squamous epithelial and urothelial (transitional) epithelial cells, which are difficult to be recognized in cytology [15]. These works and FTIR spectroscopic imaging of BC bladder have showed that various methods of sample collection, preparation, measurements and chemometric analysis can be employed to classify urine cells and bladder tissue fragments [16,17].

Our purpose is to consider the possibility of simply prepared voided urine sediments to support the BC diagnosis by FTIR spectroscopy. We intentionally investigated urine sediment, because that is a noninvasive and simplest method to collect samples containing cancer cells in the hospital condition. Urine sediment was collected from patients classified as normal, abnormal and cancer cytology. This classification was confirmed by histology of bladder sections for cases if it was possible. To bring the spectroscopic technology to the clinical field in the future, we selected the simple and rapid ATR FTIR as the best option for collection of FTIR spectra of urine sediment. Several studies have shown its suitability as a Point of Care tool (PoC) tool [18,19], demonstrating that the technique can be implemented in portable devices to be used in small clinics or field clinical trials [20], using minimum sample preprocessing [21], and providing results in a few minutes. In our work we present the correlation between mid-infrared spectra of urine sediment and routine cytology to assess if this combination could be an option for the rapid screening method for BC in a PoC scenario.

**Table 1**

The size of patient groups diagnosed according to cytology and histology. Cytological subgroup shows the assignment of 49 patients diagnosed additionally by histology to N, A, and C groups according to cytological results. Some sample exhibited the presence of microhematuria (HU) – hemolysis trace in the strip test. N – normal, A – abnormal, C – cancer, LG – low grade and HG – high grade of bladder cancer.

|                      | N  | N with<br>HU | A  | A with<br>HU | C  | C with<br>HU | LG/<br>HG |
|----------------------|----|--------------|----|--------------|----|--------------|-----------|
| Cytological groups   | 59 | 24<br>(41%)  | 50 | 26<br>(52%)  | 56 | 35<br>(63%)  | 27/<br>29 |
| Histology subgroups  | 16 | 11<br>(69%)  | 10 | 4 (40%)      | 23 | 17<br>(74%)  | 15/8      |
| Cytological subgroup | 13 | 8 (62%)      | 11 | 6 (55%)      | 25 | 18<br>(72%)  | 13/<br>12 |

## 2. Methods

### 2.1. Collection and preparation of samples with their medical assignment

The study was reviewed and accepted by the First Local Ethical Committee at the Jagiellonian University Medical College in Krakow (No. 1072.6120.100.2018).

A total number of urine samples was 165 and these samples were taken from patients with clinical suspicion of BCa. Average age was 66 years (min = 26; max = 89) and 70% of patients were men. Fresh voided urine was collected from the patient up to 30 min. after urination and an urine strip test (One + Step DUS 10, CE certificated) was performed to estimate the content of leukocytes, nitrite, urobilinogen, protein, pH, blood, S.G. density, ketones, bilirubin, and glucose. Only some samples showed the presence of microhematuria (Table 1).

To obtain cytological samples, urine was centrifuged at 2000 RPM for 5 min, spread with cytospin (Thermo Scientific Cytospin 4), fixed with 95% ethanol, and finally stained H&E (hematoxylin & eosin). Cytology was assessed according to the Paris System for Reporting Urinary Cytology [2] and patients were divided into three groups according to the presence of normal (N), abnormal (A), and cancer cells (C). All urine samples did not show in cytology non-urothelial malignancies and viral infections, which could interfere the spectroscopic analysis. Bladder wall excisions were taken from 49 patients with unclear outcomes of cytology and cystoscopy. The histological examination of the H&E-stained sections was performed according to WHO 2017 guidelines and a grading system recommended by International Society of Urological Pathology (ISUP) [22]. The size of each patient group with grading of BC is summarized in Table 1.

Photographic documentation of cytological and histological samples was recorded using an Olympus BX53 white-light microscope equipped with an Olympus DP27 digital camera.

### 2.2. FTIR data acquisition and spectral processing

The remaining fresh urine sediment was fixed with 2% glutaraldehyde and then centrifuged at 2000 RPM for 5 min. Sediment was washed with 10 ml distilled water, centrifuged (2000 RPM for 5 min.) and air-dried in a desiccator for 48 h. The 2-day delay was caused by problems with the timing of the operators involved on the measurement and was not necessary in terms of technical requirements of the method. Such prepared samples were used for ATR FTIR spectroscopic measurements with an ALPHA Bruker spectrometer equipped with a 1-reflection ATR diamond crystal. Spectra were acquired in the region of 400 – 4000  $\text{cm}^{-1}$  with a spectral resolution of 4  $\text{cm}^{-1}$ . 128 co-scans were co-added and an extended ATR correction was applied (using the routine integrated in the Bruker Opus 7.0 software). For further analysis, the 3100–800  $\text{cm}^{-1}$  region was selected. ATR FTIR spectra were firstly vector normalized in the 3100–800  $\text{cm}^{-1}$  region. Second derivative (Savitzky – Golay algorithm, 13 smoothing points) and differential FTIR

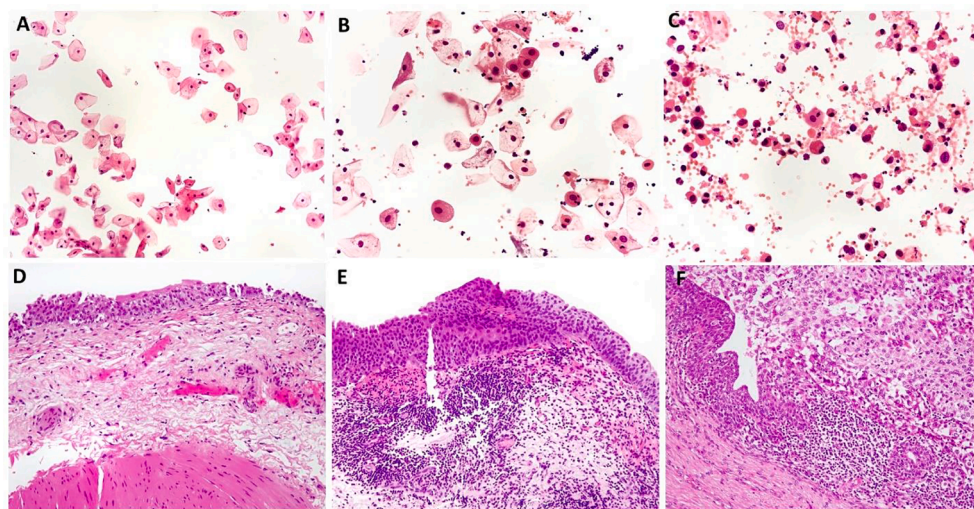


**Fig. 1.** Examples of voided urine cytology of patients from the investigated groups, (A) normal group, (B) abnormal group, and (C) – cancer group and the corresponding histological stains of bladder wall excisions, (D) normal urothelium, (E) urothelium with dysplasia, and (F) urothelial carcinoma. H&E staining; magnification: 400x (top) and 200x (bottom).

spectra were calculated and graphed in an Origin 9.1 software (ver. 2018b, OriginLab, OriginLab Corporation, Northampton, MA, USA).

Partial least squares-discriminant analysis (PLSDA) was carried out with Matlab 2020b from Mathworks (Natick, USA) and the PLStoolbox from Eigenvector (Manson, USA) functions, by using in-house written

scripts which describe the preprocessing, model selection, validation and permutation test. The scripts and datasets are available to be downloaded at the Zenodo repository (<https://doi.org/10.5281/zenodo.4587890>).

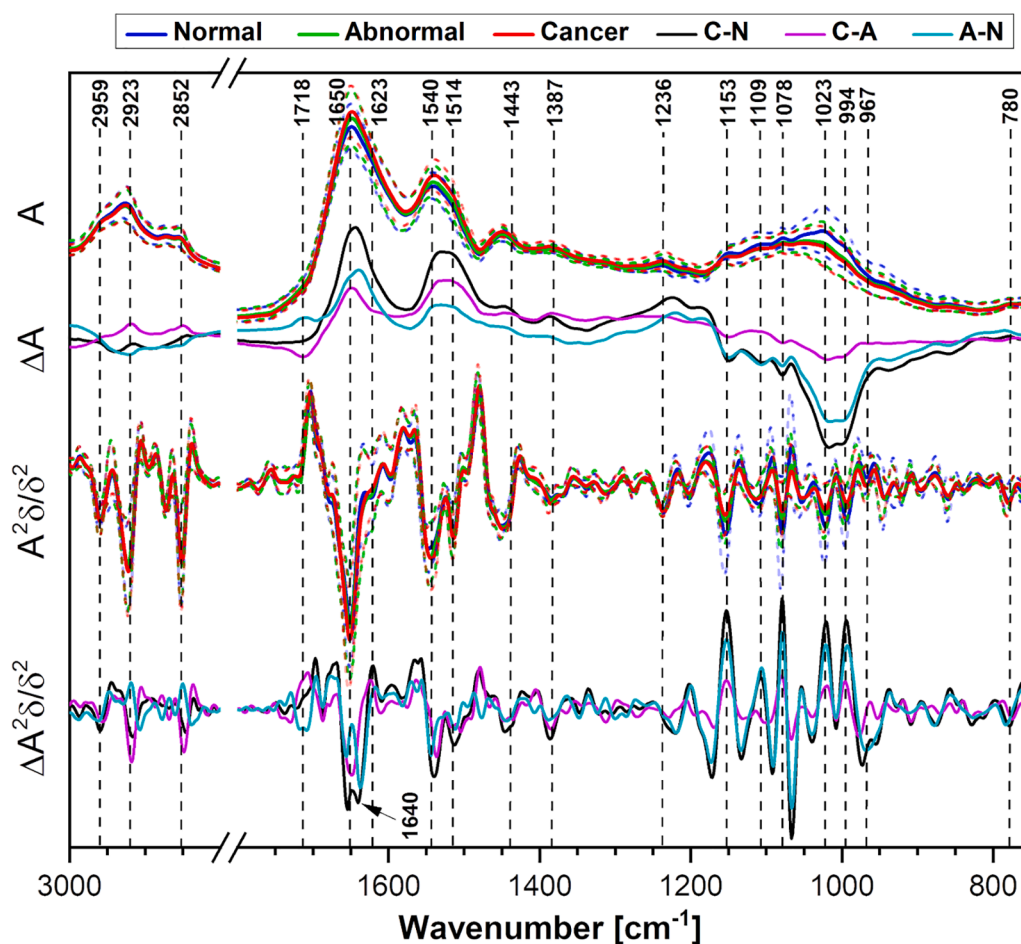


**Fig. 2.** Average absorbance and second derivative ATR FTIR spectra ( $\pm$ SD, standard deviation) of urine sediments and their differential spectra. N = 59, A = 50, C = 56 spectra.



### 3. Results and discussion

We investigated samples collected from 165 patients suspected clinically to bladder cancer. Since radiological diagnostics, ultrasonography and cystoscopy, did not revealed the presence of tumor, cytology as the best method currently used, was conducted to detect early BC (Table 1). Urine sediments were investigated spectroscopically as well. Furthermore, the patients' conditions were followed up to 6 months after the urine collection and 49 persons underwent bladder biopsy and the histological examination. The samples of these patients were redistributed in subgroups according both cytology and histology (Table 1).

#### 3.1. Morphological assessment

Cytological H&E stains for each group of patients are summarized in Fig. 1. Fig. 1A shows urine cytology of the N group with typical urothelial cells, i.e. large umbrella cells and medium-sized piriform cells from superficial and middle layers of urothelium, respectively. Both cells possess small nuclei and only few leukocytes are found. Fig. 1B and 1C display cytology of the abnormal and cancer groups, respectively, in which one can observe large and irregular circumscribed squamous cells with dark, small, and pin-shaped nuclei. Cytology from a patient with BC shows the presence of carcinomatous cells with large, irregular-shaped nuclei with hyperchromatic and coarse chromatin as well as suspicious cells, which can be classified as cancer cells (Fig. 1C). Cancer cells can be assigned to high and low grading of BC. The background is quite clear and few erythrocytes are present [2,7]. Some cells in the abnormal group exhibit a higher N/C ratio (nucleus – cytoplasm ratio) than in normal urothelial cells with a slightly irregular chromatin and nucleoli assigned to reactive changes (Fig. 1B). The A group comprises samples with degenerative, therapy-induced and reactive changes, including inflammation of normal urothelial cells and numerous leukocytes. Furthermore, atypical urothelial cells are defined when their clear assignment and morphology is not evident. Table S1 (in SI, Supporting Information) summarizes morphological features that are considered in the assignment of the patient to N, A, and C group. They include N/C ratio, hyperchromasia, irregular nuclear membrane, irregular, coarse chromatin, pleomorphism, variation of shape and size, prominent nucleoli, mitoses, necrotic debris, inflammatory cells, and cytoplasmic homogeneity. Other clinical aspects as infection, radiotherapy and surgical procedures history are also important.

The histological examination of bladder biopsies with a diameter of ca. 3–12 mm relies on the assessment of both cells' morphology and architectural tissue re-building. Normal urothelium (epithelium of bladder) should be composed of less than 5–7 layers of cells (Fig. 1D). Small cells with a high N/C ratio are localized in layers below the superficial one. Singular mitoses are possible in the basal part. Dysplasia is recognized when the stratification of urothelial cells is lost and the nucleus enlargement as well as hyperchromasia and irregular contour is observed (Fig. 1E, the left part of epithelium). BC without invasion results in remodeling of the cell stratification and nuclei have enlarged and irregular shape similarly to dysplasia, but carcinoma changes are more pronounced. Non-invasive BC could be both *in situ* (flat as in Fig. 1F) or papillary one when the papilla core contains fibrous tissue with blood vessels. The invasion means infiltration to basal lamina and further through the bladder wall to adjacent organs.

#### 3.2. Spectral differences between normal, abnormal and cancer groups assigned in cytology

The cytological assessment relies on the examination of single cells whereas spectroscopic investigations provide information about all cells in urine sediment. The number of particular cells in a sample may affect FTIR spectrum, however we decided to not count percentage of all cancer cells in the sample due to difficulties in their recognition of low grade bladder carcinoma. Fig. 2 shows average absorbance and second

**Table 2**

The most pronounced molecular changes between N, A, C groups (N = 59, A = 50, C = 56) assigned according to cytology. ↓ - decrease, ↑ - increase.

| Biomolecules  | Normal | Abnormal | Cancer |
|---------------|--------|----------|--------|
| Lipids        | ↓      | ↑        | ↑↑     |
| Proteins      | ↓      | ↑        | ↑↑     |
| Nucleic acids | ↓      | ↑        | ↑      |
| Sugars        | ↑      | ↓        | ↓↓     |

derivative ATR FTIR spectra, as well as their differential spectra for 165 patients. Band assignment is summarized in Table S2 in SI. Despite clearly visible differences in the averaged FTIR spectra, their standard deviation indicates some overlap of the spectral features which very likely result from cellular heterogeneity in the sediment. The normal urothelial cells in urine vary in function and morphology due to interactions with urine and metabolites. For instance, the basal cells proliferate to maintain epithelium, whereas the superficial cells from the upper layers build a barrier. The urine cells from healthy patients might contain glycogen or not, as it was observed by Bird et al. in FTIR spectra of single cells obtained from healthy men [15].

Differential IR spectra between C and N, C and A, and A and N groups calculated from absorbance ATR FTIR spectra indicate the main molecular differences between urine sediment (Fig. 2). Namely, samples containing BC cells possess more proteins (the 1700–1500  $\text{cm}^{-1}$  region) than the sediment with abnormal and normal urothelial cells whereas a wide region primarily assigned to sugar moieties (1200–900  $\text{cm}^{-1}$ ) shows the absorbance decrease for the cancer and abnormal groups comparing to N. A slight difference was noted between C and A groups. Differential spectra calculated for second derivative ATR FTIR spectra indicate that urine sediment with cancer cells contain more lipids than the ones with abnormal and normal cells seen in the 3000–2800  $\text{cm}^{-1}$  region in Fig. 2. Cancer and abnormal cells exhibit large N/C ratio compared to normal urothelial cells and FTIR spectra follow this feature as the 1236 and 967  $\text{cm}^{-1}$  bands of DNA are higher in the spectra of the former.

The amide I and II region show similar differences to the differential spectra calculated from the absorbance FTIR traces, but the second derivatives indicate pronounced alternations in secondary structures of proteins. Namely, the C group differs from N group by the high contribution of  $\alpha$ -helices and unordered conformations whereas the latter dominates in the abnormal group compared to normal urothelium.  $\alpha$ -Helical conformation is more pronounced in the cancer than in the abnormal group (Fig. 2). This result suggests that proteins with  $\beta$ -sheet secondary structure accompany pathological transformation of urothelial cells [23]. FTIR bands at 1153, 1078, 1023, and 994  $\text{cm}^{-1}$  assigned to glycogen are the highest in the N group and decrease gradually in abnormal and cancer groups. It is commonly known that many cells accumulate glycogen or lipids upon stress conditions or the presence of cancer cells. The urothelial cells, both with normal and cancer morphology, store carbohydrates like glycogen to synthesize carbohydrate-lipidic compounds for building glycocalyx and cerebroside based barrier, which separates the body from urine toxins [14,16,23–25]. These metabolic changes depend on the molecular background of urothelial cells and the type of bladder cancer cells [16,26]. A band assigned to uracil in RNA is progressively shifted from 1109  $\text{cm}^{-1}$  in N to 1115  $\text{cm}^{-1}$  in C. These main biocomponent differences between groups are summarized in Table 2.

#### 3.3. ATR FTIR – Based discrimination of the patient groups

PLS-DA is a multivariate analysis tool for developing a model to classify between two groups. In this work, the primary goal was a first evaluation of the potential of the technique to identify sediment from patients with BC. However, preliminary studies evidenced that the presence of A and N samples in the non-cancerous type was a

**Table 3**

Confusion matrices from the PLS DA classification of ATR FTIR spectra between C and N, C and A, and A and N groups and referred to the cytological assignment. CCR – accuracy, SN – sensitivity, SP – specificity, TP – true positive, FP – false positive, FN – false negative, TN – true negative. \*P-value obtained from the permutation test. \*\*Preprocessing used: Mean Centering (MC), Standard Normal Variate (SNV), Extended Multiplicative Standard Correction (EMSC) and First derivative (FD). \*\*\*Number of Latent Variables.

|  |   |
|--|---|
| <b>C versus N</b><br>(CCR = 68%, SN = 68%, SP = 68%, p-value*=0.01)<br>ATR FTIR classification; [SNV, FD, MC]**, 2***  | Cytological classification<br>C: 56 N: 59<br>TP: 38 FP: 19<br>FN: 18 TN: 40 |
| <b>C versus A</b><br>(CCR = 64%, SN = 66%, SP = 63%, p-value*=0.03)<br>ATR FTIR classification; [EMSC, FD, MC]**, 8*** | Cytological classification<br>A: 50 C: 56<br>TP: 33 FP: 21<br>FN: 17 TN: 35 |
| <b>A versus N</b><br>(CCR = 64%, SN = 70%, SP = 60%, p-value*=0.01)<br>ATR FTIR classification; [SNV, FD, MC]**, 9***  | Cytological classification<br>A: 50 N: 59<br>TP: 35 FP: 24                  |

confounding factor which hampered significantly the discrimination. Thus, we investigated spectral markers characteristics of each group as well as to assess the discrimination level between N and C, A and C, A and N groups. From the total ATR FTIR spectra of 165 samples, the size of each was subgroup was limited (less than 60 samples) and thus, it was impossible to create independent and representative calibration and test sets.

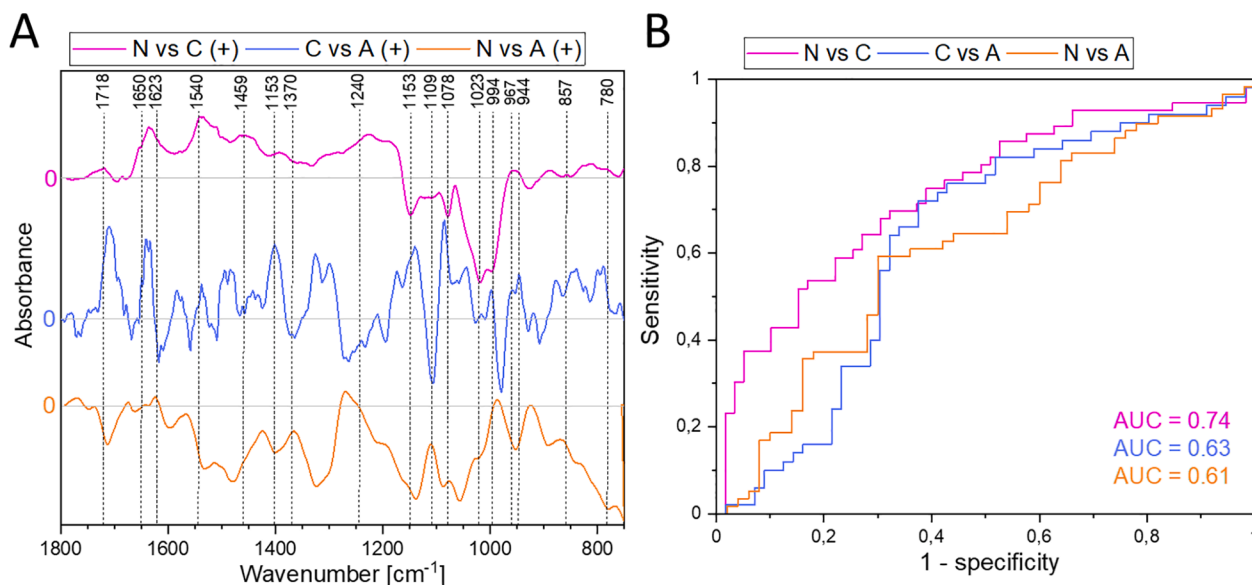
The fingerprint region ( $1800\text{--}750\text{ cm}^{-1}$ ) was considered for the modelling. The number of latent variables were chosen from a maximum of 10. The combination of different preprocessing was used, namely Standard normal variate (SNV) normalization, extended multiplicative scattering correction (EMSC) using the average spectrum of the dataset as the reference spectrum, a 15 smoothing points Savitzky – Golay first derivative (FD) and mean center. We then employed cross-validation (CV) as a measure of the classification performance of each model and investigated the regression vector for potential spectral markers. As CV error can provide over-optimistic results, we used a permutation test to ensure that the errors obtained were statistically significant.

Table 3 presents confusion matrices and their parameters obtained in the PLS DA model based on cytological classification of 165 cases. In general, classification errors range between 64 and 68%. All the errors were found significantly different by the permutation test (Wilcoxon) with p-values below 0.03 and should be put in the context of the

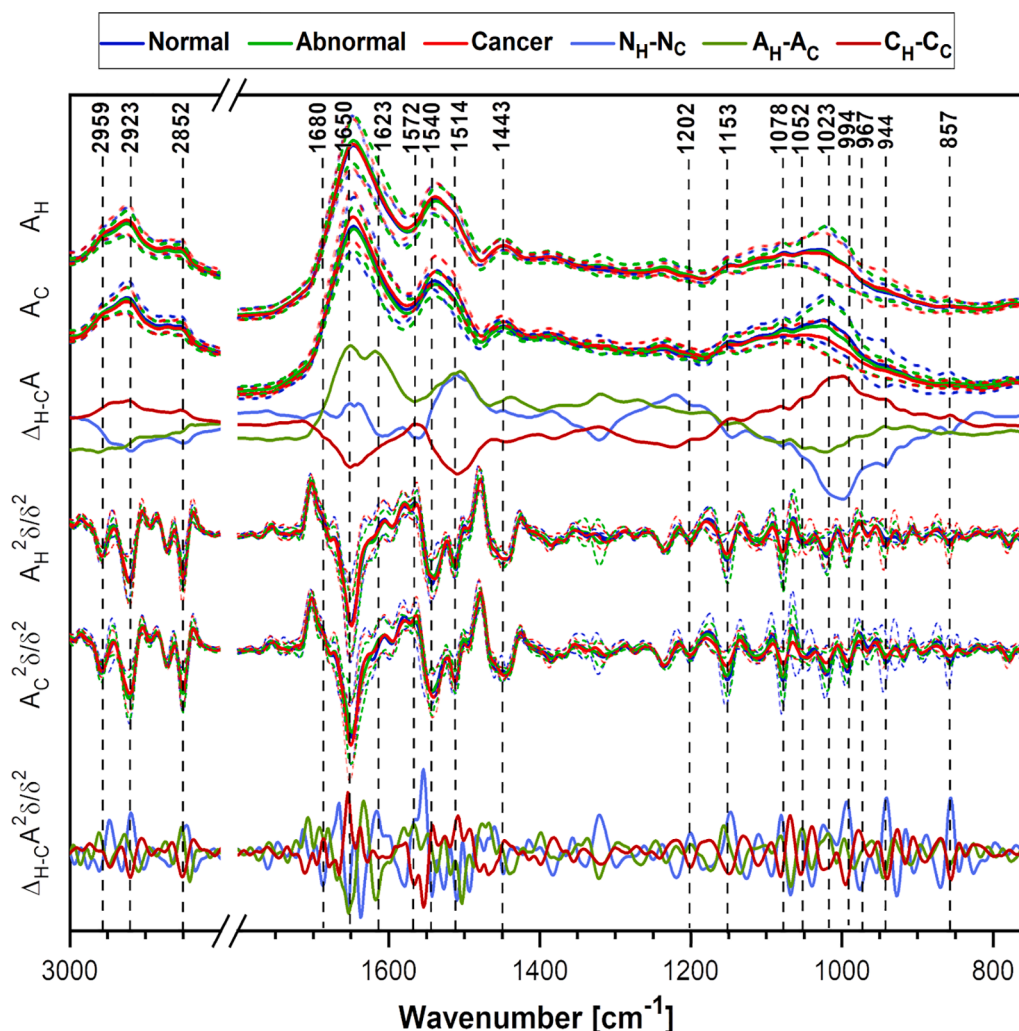
accuracy of the reference method. Indeed, the sensitivity (SN) and specificity (SP) of the ATR FTIR based model is limited by the classification performance of cytology, the method used to label the “y” of the 165 samples of the model. This technique shows a modest accuracy when compared with histological examination, the gold standard method for BC diagnosis. Here, SN and SP are max. 70 and 90%, respectively, for HG BC while SN decreases up to 30% for abnormal cells and LG BC. As accuracy, sensitivity and specificity calculated for FTIR spectral classification are 60 – 70% regardless the level of cellular abnormality, this simple, label-free and rapid method for the investigations of urine sediment shows the high capability to support the diagnosis of BC.

Fig. 3 displays regression vectors for each 2-group discrimination gathered PLS-DA with receiver operation curves (ROC). In the latter, the x-axis shows false positive rates (1-specificity) and the y-axis represents true positive rates (sensitivity). In turn, the area under the ROC curve (AUC) summarizes the overall performance of the ATR FTIR screening of urine sediment. From the leave-one-out cross validation, the AUC values are 0.74 (N vs. C), 0.63 (A vs. C), and 0.61 (A vs. N) indicating a good prediction capability, however it worsens for the abnormal cells (Fig. 3 B). Once again, we must stress here that the test method cannot provide a better performance than a the reference method to which we refer our classification.

Finally, the PLSDA models were investigated to find spectral markers responsible of the discriminations. The regression vectors of the three models are shown in Fig. 3 A. In the case of the models created using the FD, the regression vector was integrated using the function *cumsum* in Matlab. Most of them well correspond to spectral markers of the groups found in the differential FTIR spectra discussed above. In the PLS DA model for the normal versus cancer groups, positive signals of proteins and DNA at  $1640/1545/1455$  and  $1238\text{ cm}^{-1}$ , respectively assigned to the C groups are localized at) whereas strong minima in the region of  $1200 - 900\text{ cm}^{-1}$  attributed to glycogen are specific for the normal group. Regression vectors for the abnormal and cancer group depict the presence of signals at  $1368, 1270, 1100, 967\text{ cm}^{-1}$  assigned to some of carbohydrates, purines and DNA bands for C and the shift of amide I and II bands toward A. In turn vectors for the A and N pair suggests that a set of peaks assigned to lipids, carbohydrates, and RNA ( $1718, 1590, 1540, 1490, 1400, 1315, 1140, 1090, 1070, 960\text{ cm}^{-1}$ ) are specific for inflammatory and atypical cells. The fact that glycogen bands are important for the N vs. C classification in contrast to the other group



**Fig. 3.** Graphical results of PLS DA for the N, A, and C diagnosis. A present the cumulative sums of the regression vector of the discrimination ('+' – positive value of vector for marked group) and B show the receiver operation curves (ROC) for the cross validation of the patient groups.



**Fig. 4.** Average absorbance and second derivative ATR FTIR spectra ( $\pm$ SD, standard deviation) of urine sediments and their differential spectra for the histologically and cytologically assigned subgroups (in Table 1).  $N_H = 16$ ,  $A_H = 10$ ,  $C_H = 23$ ;  $N_C = 13$ ,  $A_C = 11$ ,  $C_C = 25$ .

combinations results from the ratio of healthy and cancerous cells and the number of cells exfoliated from bladder. Among BC cells high grade BC is recognized with 70% sensitivity in cytology and thus the glycogen decrease in FTIR spectra can additionally confirm a higher risk of HG BC. For the discrimination of the A and C groups, increasing absorbance of the DNA bands is in concordance with a higher N/C ratio in atypical and cancer cells resulting from a high mitotic rate and multiploidy in that cells [7]. The question arises if the strong contribution of glycogen to the discrimination of all investigated groups does not result from diabetes mellitus (DM) or low pH of urine (below 3.5) [27]. But none of the patients in our groups was diagnosed for DM and pH of urine is found in the normal range, i.e. N: 5.50 ( $\pm 0.58$ ); A: 5.25 ( $\pm 1.04$ ), and C: 5.41 ( $\pm 0.65$ ).

In the cytological diagnosis of BC patients, the main purpose is to recognize all cancer cases and their overdiagnosis is a minor issue. In suspected cases, the urologist conducts cystoscopy and eventually biopsy. Among 165 cases investigated by us, 49 patients were again diagnosed with histology (histological subgroup in Table 1). We track all samples misclassified by the ATR FTIR - PLS DA approach in the histological verification. Among 23  $C_H$  cases, 5 and only 1 patients are false negative according to cytology and ATR FTIR spectroscopy, respectively. Whilst 16  $N_H$  cases (true negative) were first cytologically classified as 4  $N_C$ , 6  $A_C$ , and 6  $C_C$ . In consequence, 75% patients underwent further unnecessary diagnostics. In turn, FTIR spectra of the sediments in this group are assigned to 7 N, 5 A, and 4 C cases. Finally, among 10  $A_H$

patients, cytology did not show any abnormalities in 4 cases whereas FTIR spectra assigned only 1 case to the normal group. This suggests that the combination of cytological and spectroscopic assignment could revise the final classification of the patient. We also note that the FTIR-based classification model should rely on the two-step verification - C vs. N and A vs. N to detect all cancer and premalignant changes.

### 3.4. Spectral differences between histological and cytological subgroups

If FTIR spectra assignment of the patients to C, A, and N groups shows a better agreement with the histological than cytological classification, the averaged spectral profiles of the groups probably differ between themselves. The two classification methods rely on the recognition of different cancer features, i.e. cytology is based on cell morphology whereas histology includes both cellular morphology and their arrangement in the bladder wall). Thus, the cytological examination often misclassifies LG BC and well detects HG BC, whereas histology is similarly sensitive to both groups of bladder carcinoma. We compare ATR FTIR spectra of the cytological and histological subgroups in Fig. 4, see also Table 1. The main spectral differences are observed in the spectral regions specific for glycogen, proteins, and lipids and exhibited as main discriminators on PLS DA, see differential spectra calculated from absorbance ATR FTIR spectra in Fig. 4 and regression vectors in Fig. 3. The  $C_H$  subgroup contains more carbohydrates and lipids and less proteins than  $C_C$  on contrary to  $N_H$  and  $N_C$ . The  $A_H$  and  $A_C$  subgroups



**Table 4**

Spectral features of the histological normal, abnormal, and cancer subgroups in comparison to cytology. ↓ - decreased, ↑ - increased, → - down-shift, ← - up-shift.

| Band [ $\text{cm}^{-1}$ ] | Normal                      | Abnormal                        | Cancer                          |
|---------------------------|-----------------------------|---------------------------------|---------------------------------|
| 2923, 2852                | ↓                           | ↑                               | → ( $4 \text{ cm}^{-1}$ )       |
| 1715–1700                 | ↓                           | ↓                               | ↑                               |
| 1680                      | ↓                           | –                               | ↑                               |
| 1650                      | ↑                           | ↓                               | –                               |
| 1640                      | ↑                           | ↑                               | ↓                               |
| 1623                      | ↓                           | –                               | –                               |
| 1202, 1078, 994           | ↓                           | –                               | ↑                               |
| 1153, 1023                | ↓                           | ↓                               | –                               |
| 1052                      | → ( $7 \text{ cm}^{-1}$ ) - | → ( $7 \text{ cm}^{-1}$ ) and ↑ | ← ( $4 \text{ cm}^{-1}$ ) and ↑ |
| 944, 857                  | ↑                           | –                               | –                               |

reveal the decrease of the sugar level with the increase of the protein content when the histological assessment is taken into consideration. The second derivative FTIR spectra and their difference indicate additionally specific bands which contribute to the observed variances between the cytological and histological subgroups (Table 4).

### 3.5. Spectral differences between low and high grade bladder cancer.

We mentioned above about the issue with the cytological recognition of low-grade bladder carcinoma. For this purpose, we compare ATR FTIR spectra of LG BC with HG BC to assess to what degree their spectral discrimination is possible. Absorbance FTIR spectra clearly show an increase of absorbances in the lipid- and carbohydrate-region, i.e.  $2959 - 2852 \text{ cm}^{-1}$  and  $1153 - 967 \text{ cm}^{-1}$  in LG BC (Fig. 5.). Since these features are specific for the abnormal group as well, ATR FTIR-based classification of LG BC might be obscured by the presence of atypical cells in

urine. However, no spectral differences in the secondary structures of proteins (the region of amide I band) on contrary to A and C groups suggest that the overall spectral profile of the urine can contribute to the grading classification.

HG bladder carcinoma is known to be more aggressive than LG. Because the histological examination of the investigated groups allows for classification of BC according to its invasiveness, we compare finally ATR FTIR spectra of urine sediments of non- and invasive carcinoma (Fig. S1 in SI). They indicate again that the higher glycogen and lipid content is specific for the non-aggressive and non-invasive BC. But the protein characteristics is different from the LG – HG BC groups.

### 3.6. Evaluation of the technique as a Point of Care tool

Although ATR-FTIR shows great potential for the PoC testing of BC, there are several challenges that should be overcome to implement the technique in the context of a community clinic, pharmacy or the doctor's office. The main impediment is the turnaround time (TAT), i.e. the time-lapse between the test and the application of the clinical treatment or response. The measurement of the spectra is performed in less than 5 min, and the computation of the result by the model from an unknown sample takes less than a second. However, the sample preprocessing involving the fixation and drying of the sample can delay the result of the test. In this regard, the drying of the samples could be easily shortened using air and heat systems. The steps of centrifugation and fixation and cleaning steps are more problematic, requiring moderate qualified staff as well as the use and disposal of reagents. These requirements may be available at some PoC locations, but limits its use on the patients home. Although the method is not far away from the PoC scenario, future efforts should focus on implementing microfluidics strategies to

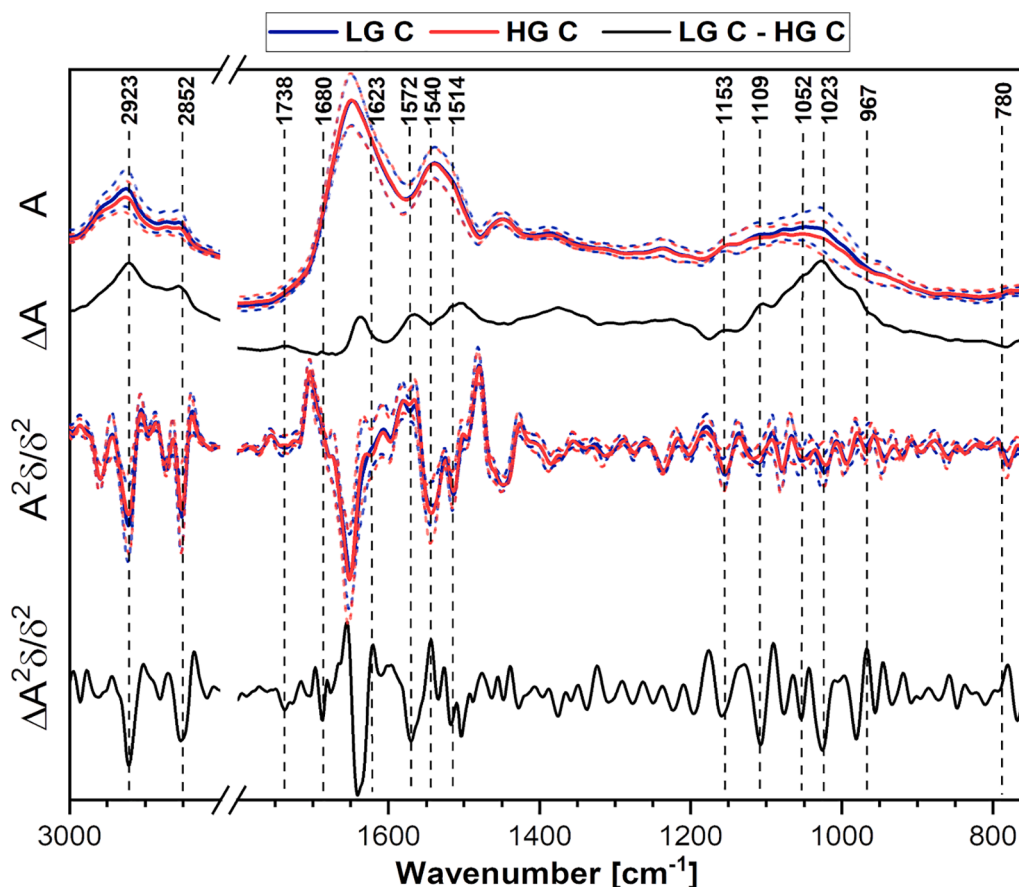


**Fig. 5.** Averaged absorbance and second derivative ATR FTIR spectra ( $\pm$ SD, standard deviation) of urine sediments and their differential spectra for low- (LG C) and high grade (HG C) bladder cancer. LG = 27, HG = 29.

provide a full PoC solution [28].

#### 4. Conclusions

In this work we proposed that ATR FTIR spectra of the urine sediment are useful for the support of the BC diagnosis. The simple urine sediment preparation and rapid and label free data collection provided the spectral markers contributing to discrimination of normal, atypical and cancer urothelial cells. The main spectral differences between the investigated groups were found in the spectral regions of glycogen, proteins and lipids. Based on that PLS-DA classification was satisfied and comparable with the cytological assessment. We pointed out that the choice of the gold reference method is crucial for the evaluation of sensitivity and specificity of the spectroscopic approach. This was reflected in the proper FTIR based re-assignment of cancer-suspected patients when they were additionally diagnosed by histology of the bladder excisions. Although the histologic diagnosis of papillary bladder carcinoma is not usually difficult for a qualified pathologist, the urine cytology is more problematic. The standard Paris criteria are focused on identifying life-threatening high-grade tumors, whereas much more frequent low-grade cancer shows minimal abnormalities at the cellular level and is very difficult to be distinguished from normal urothelial cell. The analyzed ATR FTIR spectra of the LG, HG and invasive BC suggested that the recognition of these groups is also possible. Considering the challenge of having a reference method with limited accuracy, future works should aim to perform the models using as the gold standard histology as a ground true. Further FTIR study on large group of patients diagnosed histologically could prove this hypothesis suggested by our preliminary results.

#### CRedit authorship contribution statement

**Monika Kujdowicz:** Conceptualization, Methodology, Visualization, Project administration, Funding acquisition. **David Perez Guaita:** Methodology, Writing - review & editing, Visualization, Supervision. **Piotr Chłosta:** Methodology, Writing - review & editing. **Krzysztof Okon:** Writing - review & editing, Supervision, Project administration. **Kamilla Malek:** Conceptualization, Methodology, Writing - review & editing, Project administration.

#### Declaration of Competing Interest

The authors declare that they have no known competing financial interests or personal relationships that could have appeared to influence the work reported in this paper. This project has received funding from the European Union's Horizon 2020 research and innovation programme under the Marie Skłodowska-Curie grant agreement No 796287. D.P.-G. acknowledges the financial support of the 2019 Ramón y Cajal (RYC) Contracts Aids (RYC2019- 026556-I).

#### Acknowledgement

MK thanks the National Science Centre in Poland (Preludium 16, no. UMO-2018/31/N/NZ4/00911) and the InterDokMed project (no. POWR.03.02.00-00-I013/16) for financial support.

#### Appendix A. Supplementary data

Supplementary data to this article can be found online at <https://doi.org/10.1016/j.microc.2021.106460>.

#### References

- [1] V.E.R. Holger Moch, P.A. Humphrey, T.M. Ulbright, WHO Classification of Tumours of the Urinary System and Male Genital Organs, 4th ed., 2016.
- [2] D.F.I. Rosenthal, Dorothy L., Wojcik, Eva M., Kurtzy, The Paris System for Reporting Urinary Cytology, First, Springer, 2016.

- [3] H. Vijayendra, N.H. Mahajan, V. Vijayendra, S. Ramdass, Attic retraction pockets: Classification system, Laryngoscope. 130 (8) (2020) 2034–2039, <https://doi.org/10.1002/lary.v130.810.1002/lary.28368>.
- [4] G. Santoni, M.B. Morelli, C. Amantini, N. Battelli, Urinary markers in bladder cancer: An update, Front. Oncol. 8 (2018) 1–9, <https://doi.org/10.3389/fonc.2018.00362>.
- [5] Yair Lotan Paul O'Sullivan Jay D. Raman Sharokh F. Shariat Laimonis Kavalieris Chris Frampton Parry Guilford Carthika Luxmanan James Suttie Henry Crist Douglas Scherr Scott Asroff Evan Goldfischer Jeffrey Thill David Darling 35 8 2017 531.e15 531.e22.
- [6] R. Hartman, A. Kawashima, Lower tract neoplasm: Update of imaging evaluation, Eur. J. Radiol. 97 (2017) 119–130, <https://doi.org/10.1016/j.ejrad.2017.10.019>.
- [7] R.S. Koss G. Leopold Hoda, Koss's Cytology of the Urinary Tract with Histopathologic Correlations Springer 2012.
- [8] D.F.I. Kurtzy, K.E. Sundling, G.A. Barkan, The Paris system of Reporting Urinary Cytology: Strengths and opportunities, Diagn. Cytopathol. 48 (2020) 890–895, <https://doi.org/10.1002/dc.24561>.
- [9] C.-P. Jen, C.-T. Huang, Y.-S. Chen, C.-T. Kuo, H.-C. Wang, Diagnosis of human bladder cancer cells at different stages using multispectral imaging microscopy, IEEE J. Sel. Top. Quantum Electron. 20 (3) (2014) 81–88, <https://doi.org/10.1109/JSTQE.294410.1109/JSTQE.2013.2279804>.
- [10] S.S. Chang, S.A. Boorjian, R. Chou, P.E. Clark, S. Daneshmand, B.R. Konety, R. Pruthi, D.Z. Quale, C.R. Ritch, J.D. Seigne, E.C. Skinner, N.D. Smith, J. M. McKiernan, Diagnosis and Treatment of Non-Muscle Invasive Bladder Cancer: AUA/SUO Guideline, J. Urol. 196 (4) (2016) 1021–1029, <https://doi.org/10.1016/j.juro.2016.06.049>.
- [11] D. Rodrigues, C. Jerónimo, R. Henrique, L. Belo, M. de Lourdes Bastos, P.G. de Pinho, Márcia Carvalho, Biomarkers in bladder cancer: A metabolomic approach using in vitro and ex vivo model systems, Int. J. Cancer. 139 (2) (2016) 256–268, <https://doi.org/10.1002/ijc.30016>.
- [12] M. Kujdowicz, W. Placha, B. Mech, K. Chrabaszcz, K. Okoń, K. Malek, In Vitro Spectroscopy-Based Profiling of Urothelial Carcinoma: A Fourier Transform Infrared and Raman Imaging Study, Cancers (Basel). 13 (2021) 123, <https://doi.org/10.3390/cancers13010123>.
- [13] S. Gok, O.Z. Aydin, Y.S. Sural, F. Zorlu, U. Bayol, F. Severcan, Bladder cancer diagnosis from bladder wash by Fourier transform infrared spectroscopy as a novel test for tumor recurrence, J. Biophotonics. 9 (9) (2016) 967–975, <https://doi.org/10.1002/jbio.v9.910.1002/jbio.201500322>.
- [14] S. Bensaid, A. Kachenoura, N. Costet, K. Bensalah, H. Tariel, L. Senhadji, Noninvasive detection of bladder cancer using mid-infrared spectra classification, Expert Syst. Appl. 89 (2017) 333–342, <https://doi.org/10.1016/j.eswa.2017.07.052>.
- [15] B. Bird, M.J. Romeo, M. Diem, K. Bedrossian, N. Laver, S. Naber, Cytology by infrared micro-spectroscopy: Automatic distinction of cell types in urinary cytology, Vib. Spectrosc. 48 (1) (2008) 101–106, <https://doi.org/10.1016/j.vibspec.2008.03.006>.
- [16] C. Hughes, J. Iqbal-Wahid, M. Brown, J.H. Shanks, A. Eustace, H. Denley, P. J. Hoskin, C. West, N.W. Clarke, P. Gardner, FTIR microspectroscopy of selected rare diverse sub-variants of carcinoma of the urinary bladder, J. Biophotonics. 6 (2013) 73–87, <https://doi.org/10.1002/jbio.201200126>.
- [17] C. Pezzè, A. Brunner, G.K. Bonn, C.W. Huck, Fourier transform infrared imaging analysis in discrimination studies of bladder cancer, Analyst. 138 (2013) 5719–5725, <https://doi.org/10.1039/c3an01101a>.
- [18] K.V. Oliver, F. Matjiu, C. Davey, S. Mochhala, R.J. Unwin, P.R. Rich, Attenuated total reflection Fourier transform infrared (ATR-FTIR) spectroscopy as a bedside diagnostic tool for detecting renal disease biomarkers in fresh urine samples, in, Proc. SPIE (2015), <https://doi.org/10.1117/12.2078971>.
- [19] D. Perez-Guaita, Z. Richardson, P. Heraud, B. Wood, Quantification and Identification of Microproteinuria Using Ultrafiltration and ATR-FTIR Spectroscopy, Anal. Chem. 92 (3) (2020) 2409–2416, <https://doi.org/10.1021/acs.analchem.9b0308110.1021/acs.analchem.9b03081.s001>.
- [20] P. Heraud, P. Chatchawal, M. Wongwattanakul, P. Tippayawat, C. Doerig, P. Jearanaikoon, D. Perez-Guaita, B.R. Wood, Infrared spectroscopy coupled to cloud-based data management as a tool to diagnose malaria: A pilot study in a malaria-endemic country, Malar. J. 18 (2019) 1–12, <https://doi.org/10.1186/s12936-019-2945-1>.
- [21] S. Roy, D. Perez-Guaita, D.W. Andrew, J.S. Richards, D. McNaughton, P. Heraud, B. R. Wood, Simultaneous ATR-FTIR Based Determination of Malaria Parasitemia, Glucose and Urea in Whole Blood Dried onto a Glass Slide, Anal. Chem. 89 (10) (2017) 5238–5245, <https://doi.org/10.1021/acs.analchem.6b04578>.
- [22] H. Moch, P.A. Humphrey, T.M. Ulbright, V.E. Reuter, WHO Classification of Tumours of the Urinary System and Male Genital Organs, 4th ed., International Agency for Research on Cancer, Lyon, 2016.
- [23] G.A. Bongiovanni, A.R. Eynard, R.O. Calderón, Altered lipid profile and changes in uroplakin properties of rat urothelial plasma membrane with diets of different lipid composition, Mol. Cell. Biochem. 271 (2005) 69–75, <https://doi.org/10.1007/s11010-005-4505-y>.
- [24] D. Taladrí, D. Marín, A. Alemán, I. Álvarez-Acero, P. Montero, M.C. Gómez-Guillén, Effect of chemical composition and sonication procedure on properties of food-grade soy lecithin liposomes with added glycerol, Food Res. Int. 100 (2017) 541–550, <https://doi.org/10.1016/j.foodres.2017.07.052>.
- [25] K. Brandenburg, U. Seydel, Infrared spectroscopy of glycolipids, Chem. Phys. Lipids. 96 (1–2) (1998) 23–40, [https://doi.org/10.1016/S0009-3084\(98\)00078-4](https://doi.org/10.1016/S0009-3084(98)00078-4).



- [26] B.L. Woolbright, M. Ayres, J.A. Taylor, Metabolic changes in bladder cancer, *Urol. Oncol. Semin. Orig. Investig.* 36 (7) (2018) 327–337, <https://doi.org/10.1016/j.urolonc.2018.04.010>.
- [27] C. Paulo, J. Kenney, P. Persson, M. Dittrich, Effects of phosphorus in growth media on biomineralization and cell surface properties of marine cyanobacteria *synechococcus*, *Geosci.* 8 (12) (2018) 471, <https://doi.org/10.3390/geosciences8120471>.
- [28] R. Gorkin, J. Park, J. Siegrist, M. Amasia, B.S. Lee, J.M. Park, J. Kim, H. Kim, M. Madou, Y.K. Cho, Centrifugal microfluidics for biomedical applications, *Lab Chip.* 10 (2010) 1758–1773, <https://doi.org/10.1039/b924109d>.